JOURNAL OF SYNCHROTRON RADIATION

Volume 26 (2019)

Supporting information for article:

Multi-element Effects on Arsenate Accumulation in a Geochemical Matrix Determined Using μ-XRF, μ-XANES, and Spatial Statistics

Aakriti Sharma, Amanda Muyskens, Joseph Guinness, Matthew Polizzotto, Montserrat Fuentes, Ryan Tappero, Yu-chen Chen-Wiegart, Juergen Thieme, Garth Williams, Alvin Acerbo and Dean Hesterberg

Table of Contents

Additional Methods

μ-X-ray Fluorescence Imaging and Peak Fitting for Data Collected on the SRX Beamline. X-ray fluorescence images across ROI-100 were acquired on the SRX Beamline (5-ID) at NSLS-II, Brookhaven National Laboratory in Upton, NY to assess the spatial distribution of matrix elements and accumulated As in the sand-grain surface coating. The incident energy was 13.5 keV and the nominal beam spot size was ~1 μm x 1 μm, controlled by a Si(111) monochromator and Kirkpatrick-Baez (KB) mirrors. The synchrotron ring current was constant at 150 mA. Following are details of μ-XRF image acquisition.

Detector set up. A three-element, Vortex silicon drift detector was set at an angle of ~ 87° relative to the incident beam (close to the optimal 90°) to minimize the elastic scattering signal. Also, the sample stage itself was rotated by ~13° away from a position perpendicular to the beam to decrease surface topography effects on the fluorescence signal, at the expense of an elongation of the beam spot along the x-axis of the sample. To further minimize scattering due to the uneven topography of the sand grain surface, the height of the detector was adjusted until all three detectors measured similar fluorescence signals at 13.5 keV incident energy.

Assessing elemental spatial distribution. A thinly coated 100 μm x 100 μm region (ROI-100) was selected on the surface of the sand grain using an optical microscope. To initially assess fluorescence signal intensities from soil matrix elements, a coarse navigation image was collected across ROI-100 by step scanning with a 2.5 μm step size and 0.5 s dwell time at an incident-beam energy of 13.5 keV. ROI-100 was imaged prior to treatment with As(V) to ensure minimal As background and to assess the initial spatial distribution of matrix elements. Images were acquired by raster scanning in step-scan mode at 13.5 keV using 0.5 μm step size, and 0.5 s dwell time. The grain was then treated with pH 5, 0.1 mM aqueous KH_2AsO_4 solution as

described in the main text, remounted, and the alignment was refined statistically in post-processing (discussed in the main text). Images were recollected on ROI-100 after treatment with As(V) solution using the same parameters used for acquiring images before treatment.

***Detector Multi-channel Analyzer (MCA) spectrum fitting*.** We observed differences between fluorescence signals received by each of the three Vortex silicon-drift detector elements, presumably because of natural topographic roughness of the non-polished sand grain surface at ROI-100. Signals from two of the detector elements were unreliable, therefore we did not merge data from the three elements. We used the fluorescence data from only one detector element for analysis. To separate fluorescence signals from individual chemical elements, the signals from all pixels in ROI-100 were summed to enhance those from low-concentration elements, and a model was fit to the summed full detector spectrum using the software package PyXRF (Li *et al.*, 2017). This model was then fit to the spectra from individual pixels to produce images of each element of interest.

μ-X-ray Fluorescence Imaging for μ-XANES Spectroscopy on the XFM Beamline. X-ray fluorescence images across ROI-200 were acquired on the XFM Beamline (4-BM) at NSLS-II, Brookhaven National Laboratory in Upton, NY to select spots for As K-edge μ-XANES. The nominal beam spot size was 2 μm x 2 μm, and the beam current was constant at 400 mA. The incident energy and the beam spot size was controlled by a Si(111) monochromator and Kirkpatrick-Baez (KB) mirrors. Following are details of μ-XRF image acquisition.

***Detector set up*.** A four-element, Vortex silicon-drift detector was set at an angle of 45° relative to the sample to yield maximum fluorescence signals.

Assessing elemental spatial distribution. To create an image on the XFM beamline that included ROI-100 imaged at the SRX beamline, coarse navigation images of Fe and As that was four times larger than ROI-100 were collected based on physical features visible on the sand grain with a light microscope. The location of ROI-100 was refined by comparing features in µ-XRF-images from both beamlines, then, a 200 µm x 200 µm µ-XRF image (ROI-200) of Fe and As that encompassed ROI-100 was collected (Fig. A.2) to select spots for µ-XANES analysis. The images at the XFM beamline were created at 12.7 keV incident X-rays with 3 µm step size and 1 sec dwell time. The fluorescence spectra from a multichannel analyzer were converted to element-specific fluorescence intensities at each image pixel using the software package Larch, with 300 eV windows bracketing known Kα fluorescence energies of each element (GitHub, 2018).

Collecting Arsenic K-edge µ-XANES Spectra. The µ-XANES spectra were collected across ROI-200 and ROI-10b as point XANES at energies between 11767 and 12117 eV, using a 2 µm step size and 10 s dwell time at each energy. Energy step sizes were 5 eV between 11767 and 11852 eV (baseline), 0.5 eV between 11852 and 11882 eV (edge region), 1 eV between 11882 and 11917, 2 eV between 11917 and 11997, and 5 eV between 11997 and 12117 eV.

Linear Combination Fitting (LCF) Analysis of Arsenic K-edge µ-XANES Spectra. Arsenic K-edge µ-XANES spectra were fit to develop speciation models for accumulated As analyzed at the NSLS-II XFM Beamline across both ROI-200 (6 spectra) and ROI-10b (25 spectra). The spectra were normalized as described in the main text. The two approaches to LCF analyses described next were performed using IFEFFIT under the Athena interface (Ravel & Newville, 2005) at various stages of modeling the sets of 6 or 25 µ-XANES spectra.

I. Modified Manceau Approach: In this standard elimination approach, a given sample spectrum was fit simultaneously with spectra from all 12 standards, allowing both positive and negative proportions of standards with no energy shifts allowed on the sample or standards. The standard spectra fit with the most negative proportion was removed from the set, and the sample was fit again with the remaining standards. This standard-elimination process was repeated, each time eliminating the standard that had the most negative proportion (or in some cases, least positive proportion less than ~5%) until a final set of standards (typically 2 or 3) with proportions ≥5% fit the sample. To create a "reference fit", these final standards were again used, but a maximum energy shift of ±0.25 eV (one-half of the energy step size across the edge) was allowed on each standard to account for any minor calibration errors between beamlines. If the calculated energy shift for any standard was greater than ±0.25 eV, then the shift for that standard was set at the ±0.25 eV limit. A sequence of fits allowing ±0.25 eV energy shift was then performed by individually re-introducing each of the previously eliminated standards into the LCF analysis to seek a global best fit based on a minimum residual (R-factor in Athena) taken as the goodness-of-fit parameter. If a re-introduced standard yielded a positive coefficient ≥5% and improved the R-factor of the fit by >10% relative to the reference fit or a previously better fit, then that standard was included in the set, any standards with <5% coefficient were eliminated, and all other standards were re-evaluated until a final fit with minimum R-factor (within 10%) was obtained with all standards contributing ≥5% to the overall sample fit. Weighting factors on fitting standards were not constrained, but were re-normalized to sum to 100% (Kelly *et al.*, 2008). The typical sum of weights on standards in fits to six μ-XANES spectra from ROI-200 and spectra from ROI-10b ranged from 91% to 104% and 95% to 125%, respectively, before renormalizing to 100%.

II. Combinatorics: Samples were also fit with all possible combinations (combinatorics) of up to three standards (286 fits total with 12 standards) as a consistency check on the modified Manceau approach for the set of six µ-XANES spectra from ROI-200, and as a secondary approach for selecting a subset of standards and constraining energy shifts in fitting the 25 µ-XANES spectra from ROI-10b. In the combinatorial approach, unconstrained energy shifts were allowed for individual standards, but only fits in which all standards had proportions >10% and shifted by less than ±0.25 eV were considered acceptable fits. Weighting factors on fitting standards were constrained to be positive only, but were not constrained to sum to one. Standards in fits that had R-factors ≤10% greater than the fit with the lowest R-factor for a given sample spectrum were considered to be viable standards for modeling the data. Ultimately, both LCF approaches yielded the same sets of standards as being viable for each sample spectrum from ROI-200 and each of the four merged spectra for Fe quartiles in ROI-10b. Moreover, the mean energy shifts in combinatoric fitting to the two final standards selected from both LCF approaches applied to merged, quartile spectra from ROI-10b were -0.17± 0.29 (n = 24) and -0.45 ± 0.1 (n = 27) for As(V)-ferrihydrite co-ppt and As(V)-boehmite standards, respectively. Consequently, when fitting the 25 individual µ-XANES spectra from ROI-10b, we fixed the energy shifts of these two standards at 0 and -0.45 eV for all fits to assess variations in spectra across the 10 µm x 10 µm spatial domain based on proportions of standards and goodness-of-fit (R-factors) only, without confounding effects of minor energy shifts on the standards.

Table S1. Arsenic standards used in linear-combination fitting analysis of As μ-XANES spectra.

Abbreviations used for arsenic standards	Description of arsenic standards
Standard spectra collected on the bulk beamlines	
1. As(V)-ferrihydrite (adsorbed)	As(V) as KH_2AsO_4 adsorbed on ferrihydrite at pH 5.5 at 1200 mmol As/kg
2. As(V)-goethite	As(V) sorbed onto goethite in the presence of artificial river water (ARW) at 4222 mg/kg. The ARW consists 1.29 mM NaCl, 0.09 mM KCl, 0.49 mM $CaCl_2$, and 0.34 mM $MgSO_4$.
3. As(V)-Fe-peat	KH_2AsO_4 bound to hydrated and acid washed Pahokee peat reacted with 2400 mmol Fe/kg at pH 5.5; As(V) added at 1200 mmol/kg
4. As(V)-boehmite	As(V) as KH_2AsO_4 adsorbed on poorly crystalline boehmite at pH 6 at 50 mmol As/kg
5. Scorodite (bulk)	Scorodite diluted in BN to 850 mmol As/kg
6. As(III)-Fe-peat	As(III) as KH_2AsO_3 bound to hydrated and acid-washed Pahokee peat reacted with 2400 mmol Fe/kg at pH 5.5; As(III) added at 200 mmol/kg
7. As(V) oxide	As_2O_5 diluted in BN to 850 mmol As/kg
8. Mansfieldite	Mansfieldite diluted in BN to 850 mmol As/kg
9. Dimethylarsinic acid	Dimethylarsinic acid $(CH_3)_2As(O)OH$, diluted in BN to 850 mmol As/kg
10. Ca-arsenate	Ca arsenate $Ca_3(AsO_4)_2$ diluted in BN to 850 mmol As/kg
Standard spectra collected along with the samples on the XFM beamline	
11. As(V)-ferrihydrite (co-ppt)	As(V) co-precipitated with ferrihydrite at 0.1 mol As/mol Fe
12. Scorodite (micro)	Scorodite inclusion in a rock sample

Table S2. Linear combination fitting results showing combinations of two standards [As(V) co-precipitated with ferrihydrite or adsorbed on boehmite] fit to individual As μ-XANES spectra collected from ROI-10b, with spot numbers ordered from right-to-left starting at the bottom row (fits are overlaid on data in Fig. 5 of the main text).

Spot #	Quartile†	Proportions of standards ± uncertainty		R-factor
		As(V)-ferrihydrite (co-ppt)	As(V)-boehmite (adsorbed)	
1	ML	70 ± 7	30 ± 7	0.0105
2	L	71 ± 12	29 ± 12	0.0167
3	L	47 ± 10	53 ± 10	0.0157
4	L	66 ± 11	34 ± 11	0.0191
5	L	59 ± 10	41 ± 10	0.0179
6	MH	84 ± 6	16 ± 6	0.0070
7	ML	55 ± 8	45 ± 8	0.0077
8	ML	36 ± 10	64 ± 4	0.0154
9	L	65 ± 13	35 ± 13	0.0177
10	L	77 ± 11	23 ± 11	0.0219
11	H	84 ± 6	16 ± 6	0.0065
12	MH	65 ± 6	35 ± 6	0.0070
13	ML	68 ± 8	32 ± 8	0.0109
14	ML	49 ± 4	51 ± 4	0.0128
15	ML	71 ± 14	29 ± 14	0.0242
16	H	95 ± 0	5 ± 0	0.0075
17	H	81 ± 6	19 ± 6	0.0052
18	MH	70 ± 6	30 ± 6	0.0066
19	MH	74 ± 7	26 ± 7	0.0077
20	ML	73 ± 6	27 ± 6	0.0067
21	MH	58 ± 6	42 ± 6	0.0055
22	H	76 ± 5	24 ± 5	0.0040
23	MH	64 ± 5	36 ± 5	0.0034
24	H	70 ± 6	30 ± 6	0.0056
25	H	39 ± 6	61 ± 6	0.0043

† Quartiles: H = high, MH = medium high, ML = medium low, L = low

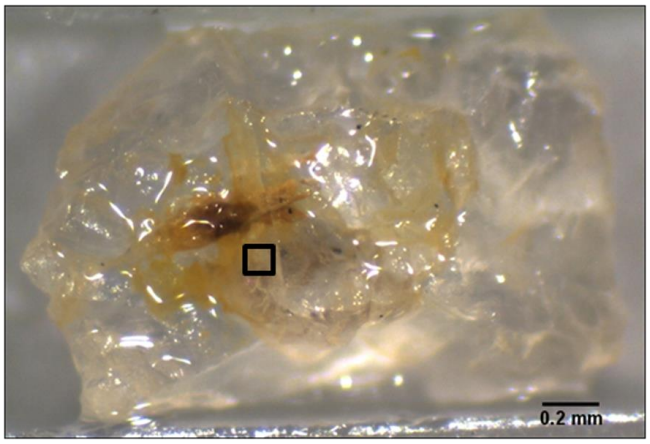

Figure S1. Light-microscope image of the quartz sand-grain fractionated from an Ultisol soil sample and analyzed in this study. Brownish-colored regions reflect grain coatings containing Fe(III)-oxides. The black box shows the 100 µm x 100 µm region of interest (ROI-100) from which µ-XRF and µ-XANES data were collected.

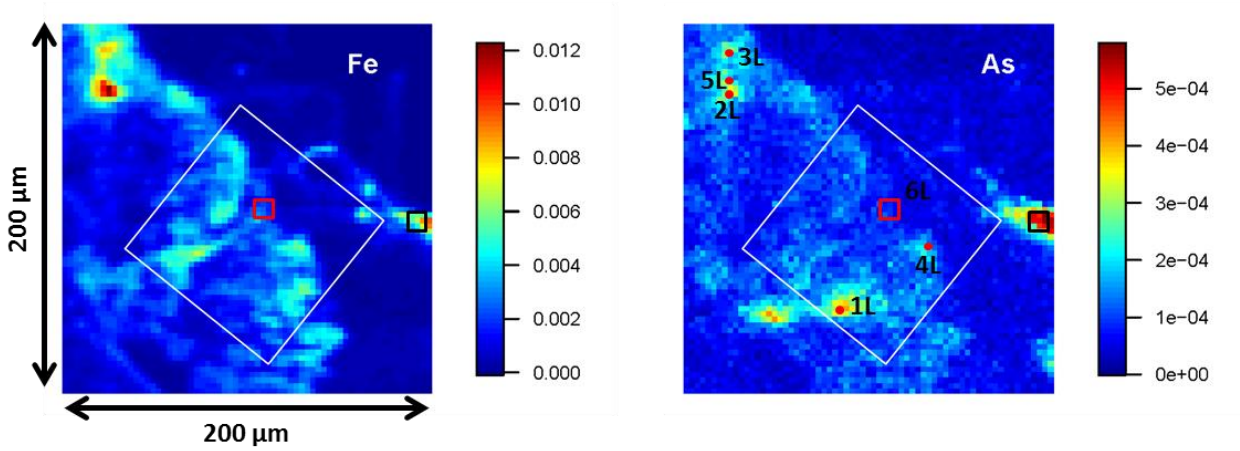

Figure S2. Micro-XRF images of Fe and As created across ROI-200 on the XFM beamline to select pixels for collecting As µ-XANES spectra. Brighter colors indicate greater elemental fluorescence signals. The white square shows the approximate region of ROI-100 based on the crescent-shaped pattern of higher Fe signal near the top corner of the box, which appears to correspond with a similar pattern visible in the Fe image collected across ROI-100 (Fig. 1) on the SRX beamline. The red dots and the square are the regions where As µ-XANES spectra were collected. The black square shows ROI-10b, which was selected to determine whether multi-element heterogeneity of soil microsites affects As speciation.

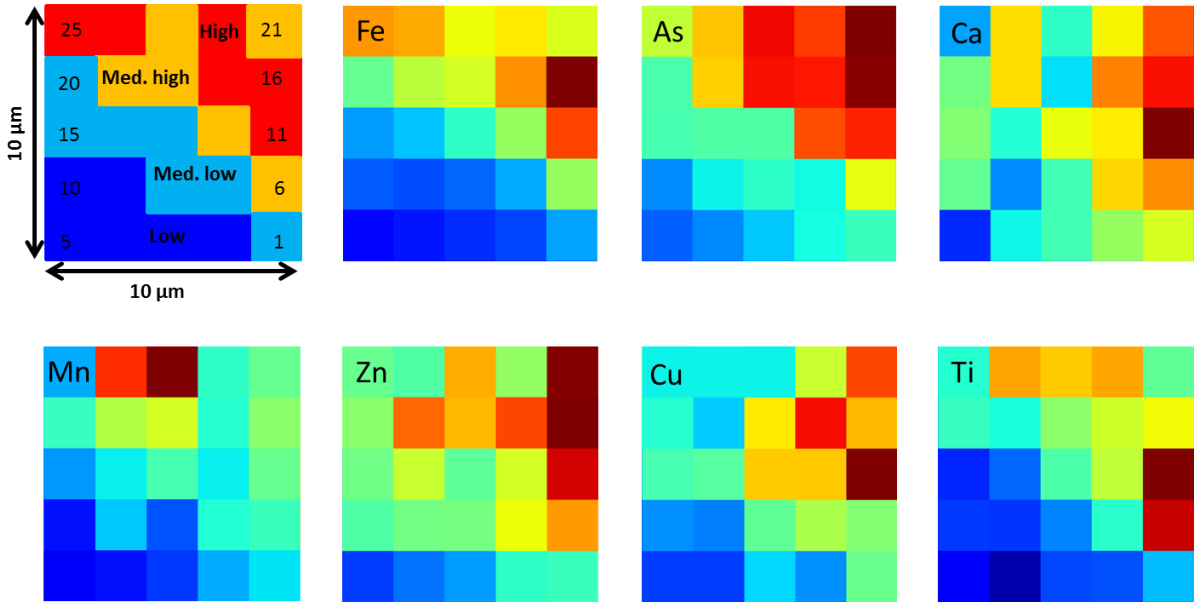

Figure S3. Micro-XRF images of all elements collected across ROI-10b, a region that showed spatial variability of the elements imaged, on the XFM beamline. The top left image delineates by color pixels belonging to each quartile of Fe fluorescence signals (high, medium high, medium low, and low). Brighter colors in the elemental images indicate greater I_0-normalized fluorescence intensities, with maximum intensities of 0.00882 (Fe), 0.00057 (As), 0.00018 (Ca), 0.00038 (Mn), 0.00026 (Zn), 0.00025 (Cu), and 0.00051 (Ti).

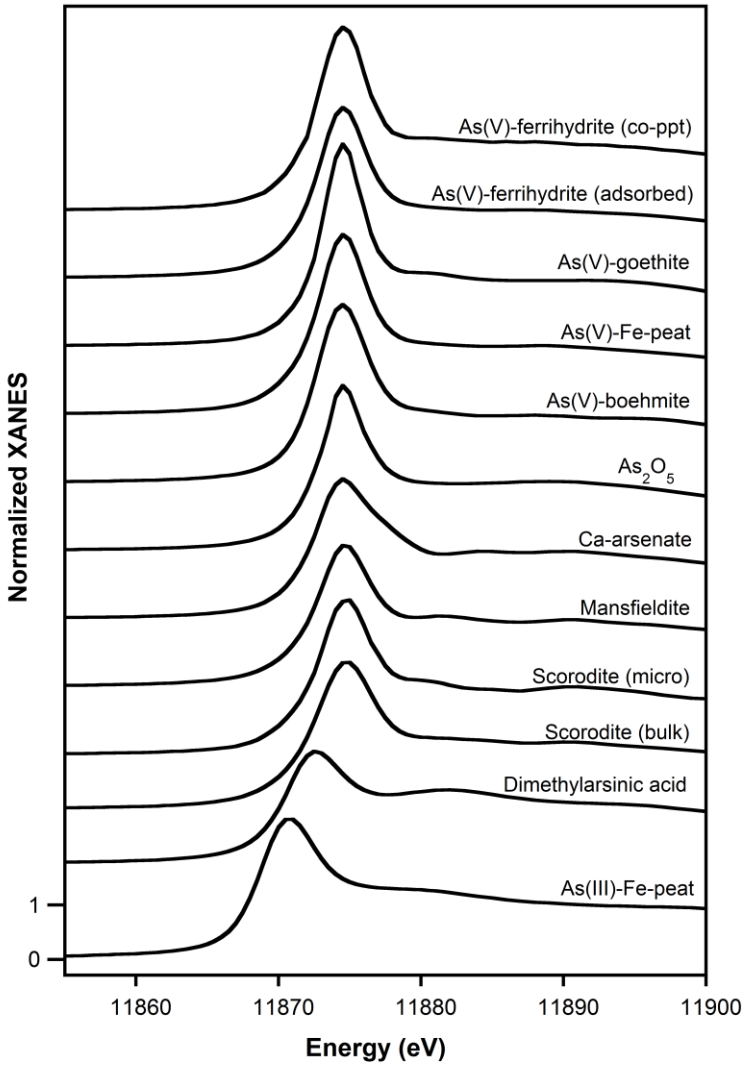

Figure S4. Arsenic K-edge XANES spectra for standards used in linear combination fitting analysis.

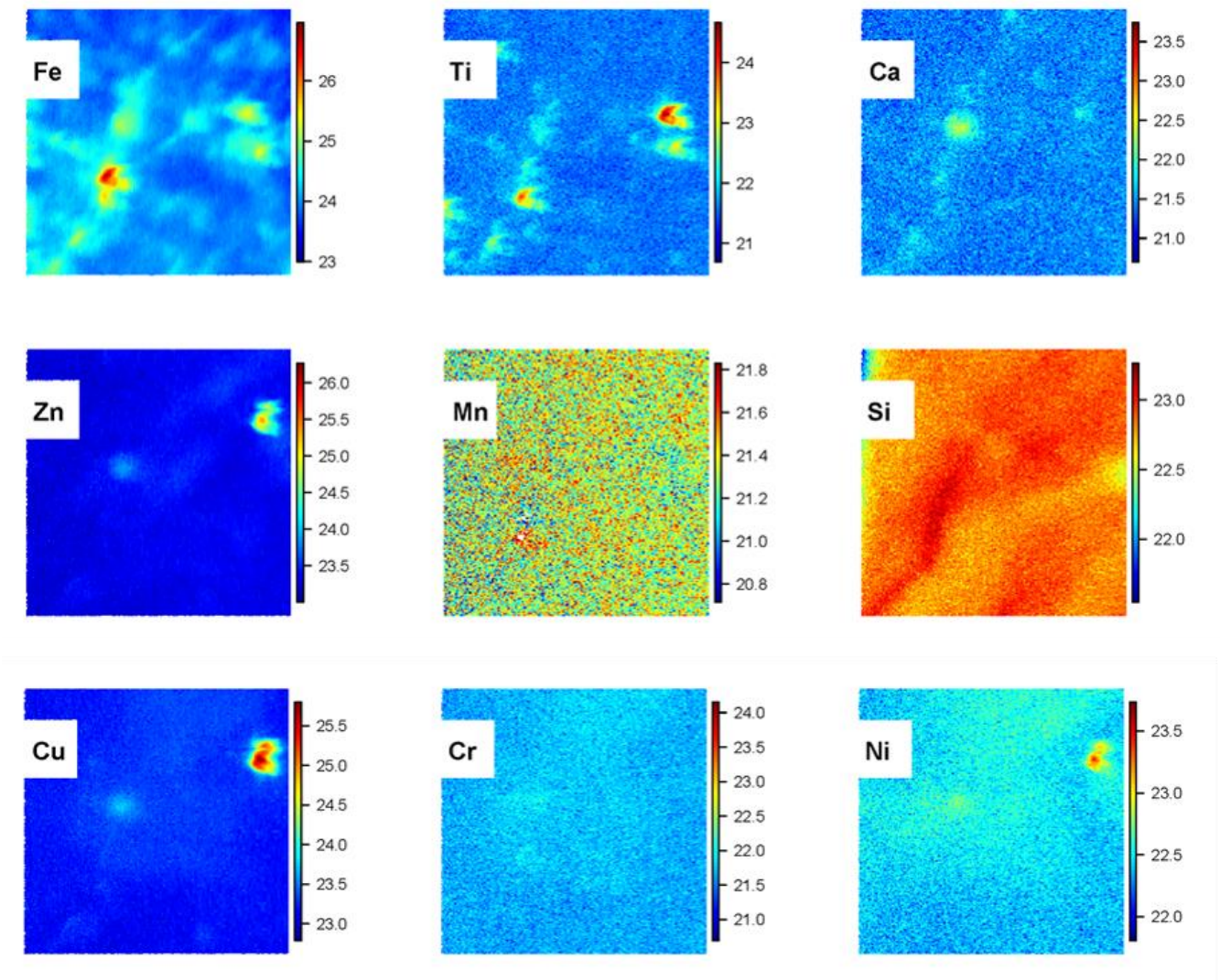

Figure S5. Micro-XRF images of selected soil-matrix elements collected across ROI-100 of the studied sand grain after the treatment with 0.1 mM As(V) solution. Brighter colors indicate greater elemental fluorescence signals on natural log-transformed data. Element labels are placed on a region of the image with missing data.

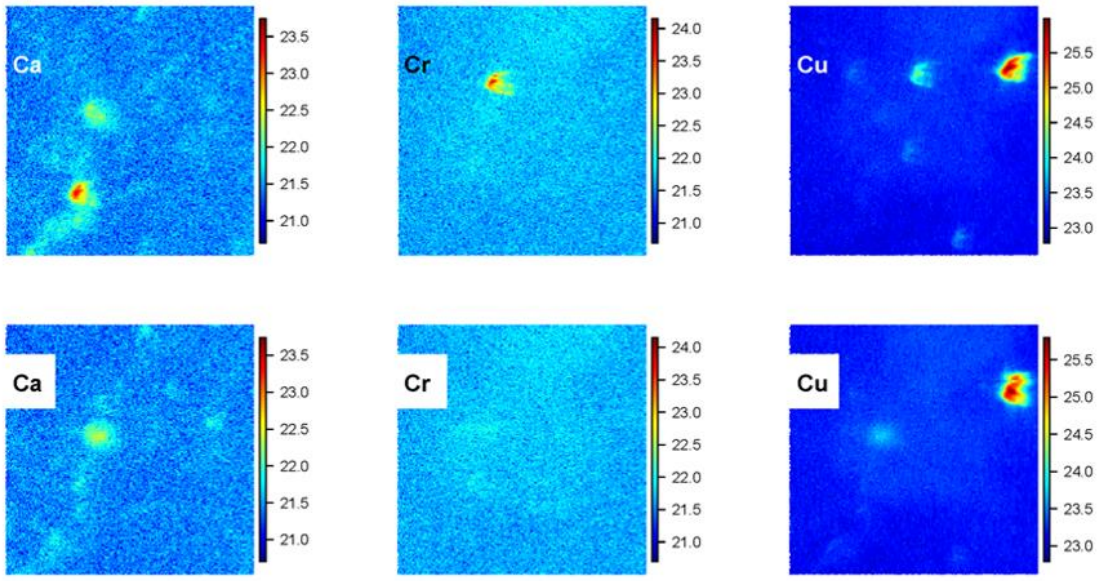

Figure S6. Micro-XRF images of Ca, Cr, and Cu collected across ROI-100 of the studied sand grain before (top) and after (bottom) treatment with 0.1 mM As(V) solution showing changes in measured spatial patterns. Brighter colors indicate greater elemental fluorescence signals on natural log-transformed data.

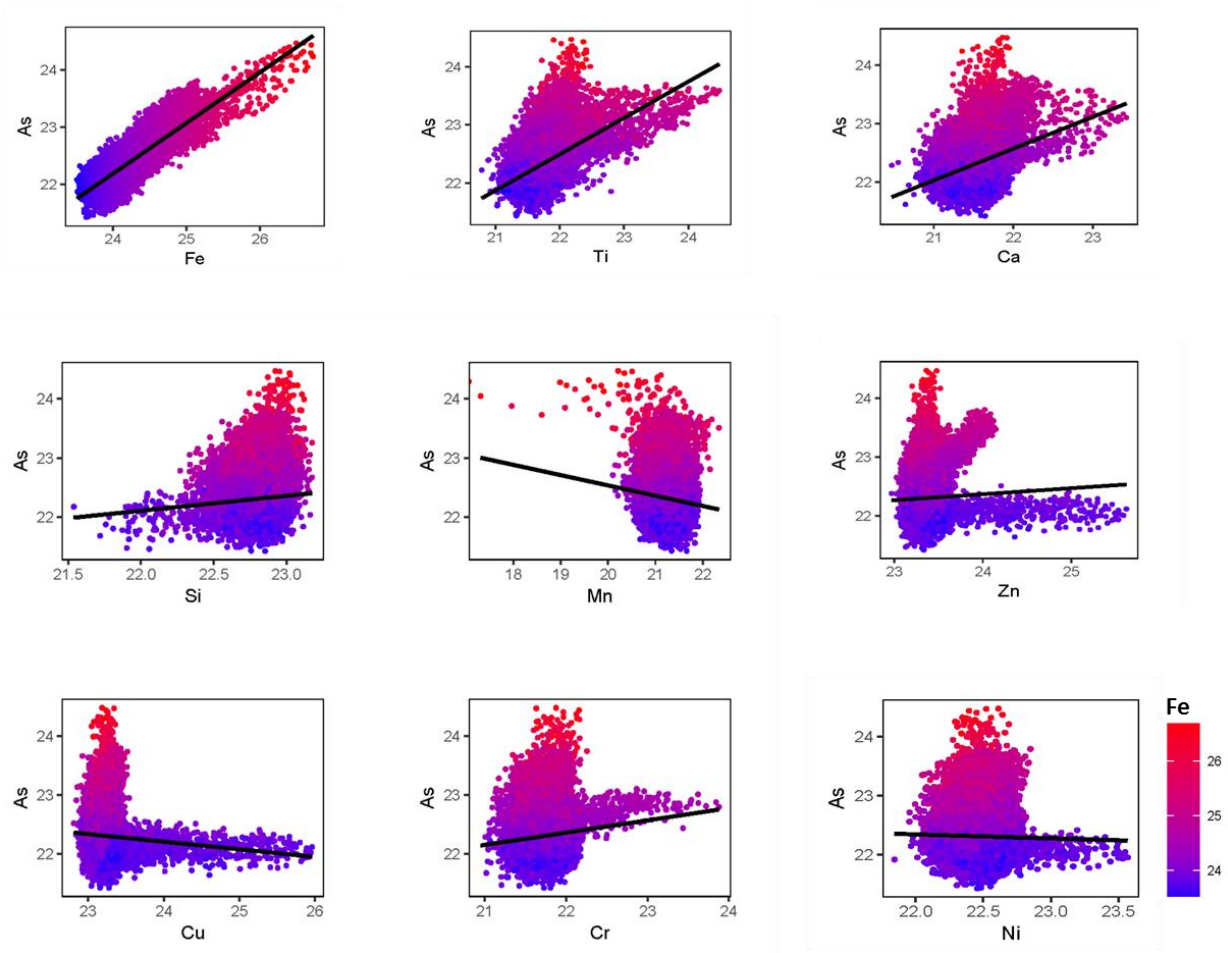

Figure S7. Scatter plots of natural log-transformed μ-XRF intensities of As vs. detected matrix elements from ROI-100 of the studied sand grain. Data points are colored according to the Fe fluorescence intensity shown in the scale bar. These scatter plots showed the maximum accumulation of As in the regions of high Fe, rather than where Ti, Ca, or other elements were high, suggesting that the effect of other elements on As accumulation is governed by Fe.

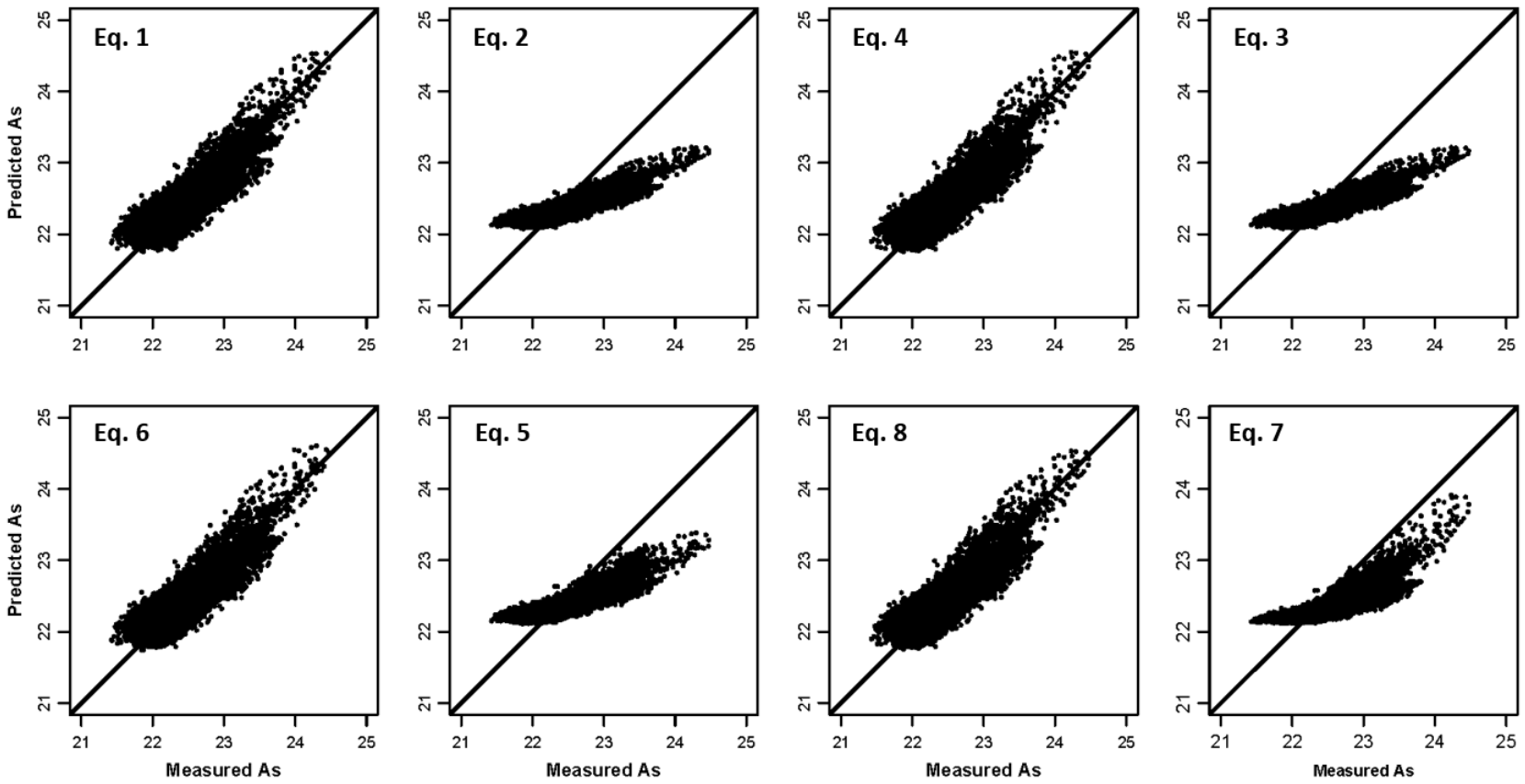

Figure S8. Scatter plots of predicted vs measured natural log-transformed arsenic μ-XRF signals for non-spatial and spatial predictive models developed for ROI-100 shown in Table 2, and 1:1 lines are plotted to compare predictions.

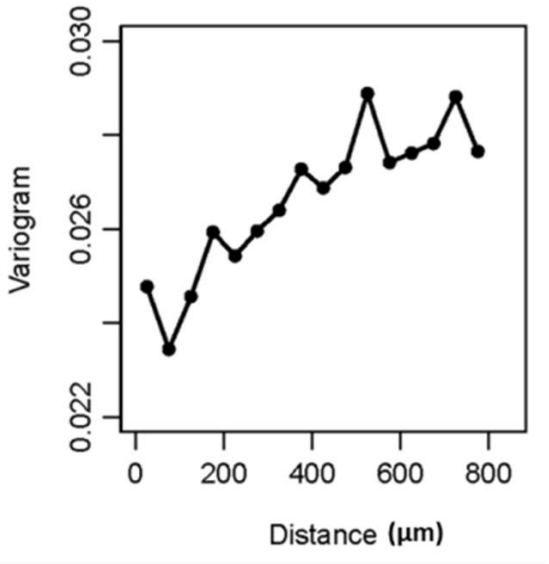

Figure S9. Average empirical variogram plot of residuals from Eq. 1 showed spatial dependence.

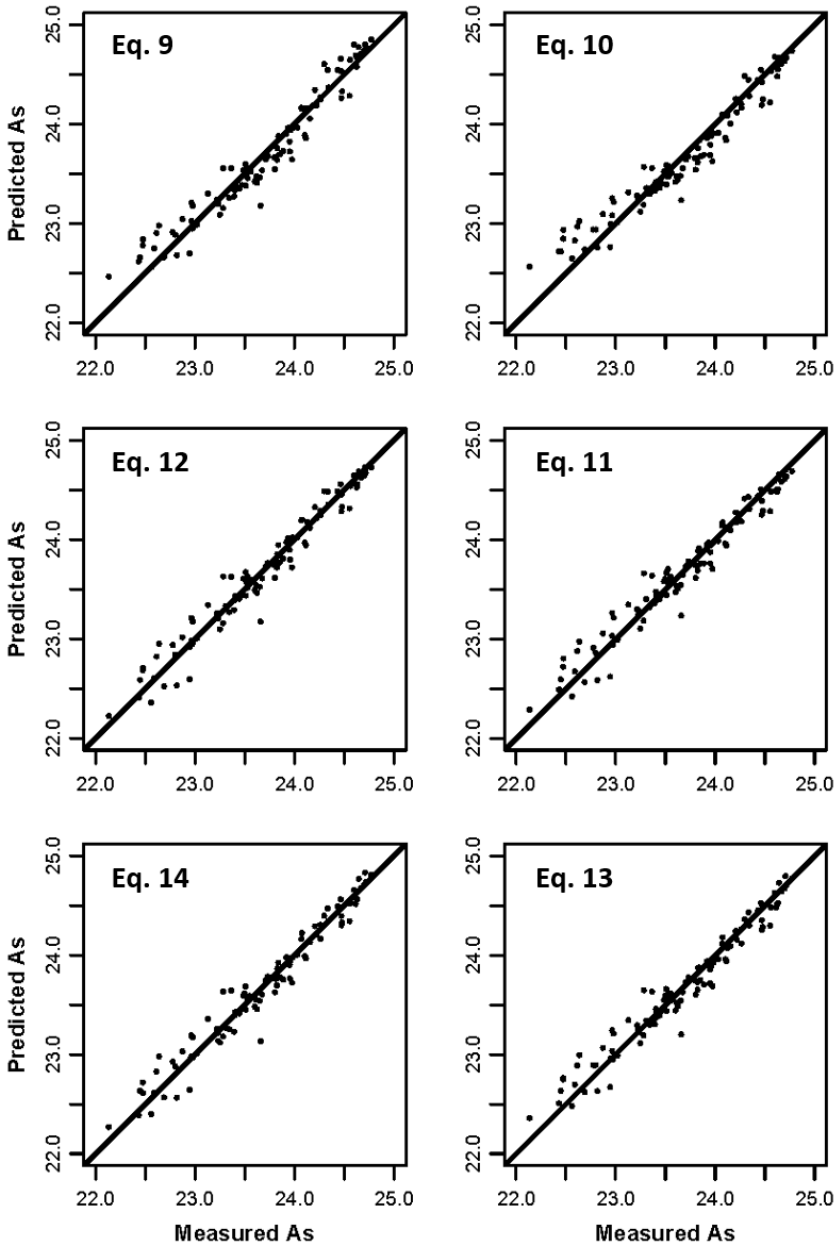

Figure S10. Scatter plots of predicted vs measured natural log-transformed arsenic μ-XRF signals for non-spatial and spatial predictive models developed for ROI-10a shown in Table 3, and 1:1 lines are plotted to compare predictions.

References Cited in Supporting Information

GitHub, I. (2018). *Larch: X-Ray Analysis for Synchrotron Applications Using Python*, https://github.com/xraypy/xraylarch.

Kelly, S., Hesterberg, D. & Ravel, B. (2008). *Methods of soil analysis. Part 5* 387-464.

Li, L., Yan, H., Xu, W., Yu, D., Heroux, A., Lee, W.-K., Campbell, S. I. & Chu, Y. S. (2017). *X-Ray Nanoimaging: Instruments and Methods III*, p. 103890U. International Society for Optics and Photonics.

Ravel, B. & Newville, M. (2005). *J. Synchrotron Radiat.* **12**, 537-541.